Escherichia coli dihydrofolate reductase catalyzed proton and hydride transfers: Temporal order and the roles of Asp27 and Tyr100

C. Tony Liu[a,1], Kevin Francis[b,1], Joshua P. Layfield[c], Xinyi Huang[a], Sharon Hammes-Schiffer[c], Amnon Kohen[b,2], and Stephen J. Benkovic[a,2]

[a]Department of Chemistry, Pennsylvania State University, University Park, PA 16802; [b]Department of Chemistry, The University of Iowa, Iowa City, IA 52242; and [c]Department of Chemistry, University of Illinois at Urbana–Champaign, Urbana, IL 61801-3364

Edited by Gregory A. Petsko, Weill Cornell Medical College, New York, NY, and approved October 30, 2014 (received for review August 18, 2014)

The reaction catalyzed by *Escherichia coli* dihydrofolate reductase (*ec*DHFR) has become a model for understanding enzyme catalysis, and yet several details of its mechanism are still unresolved. Specifically, the mechanism of the chemical step, the hydride transfer reaction, is not fully resolved. We found, unexpectedly, the presence of two reactive ternary complexes [enzyme:NADPH:7,8-dihydrofolate (E:NADPH:DHF)] separated by one ionization event. Furthermore, multiple kinetic isotope effect (KIE) studies revealed a stepwise mechanism in which protonation of the DHF precedes the hydride transfer from the nicotinamide cofactor (NADPH) for both reactive ternary complexes of the WT enzyme. This mechanism was supported by the pH- and temperature-independent intrinsic KIEs for the C-H→C hydride transfer between NADPH and the preprotonated DHF. Moreover, we showed that active site residues D27 and Y100 play a synergistic role in facilitating both the proton transfer and subsequent hydride transfer steps. Although D27 appears to have a greater effect on the overall rate of conversion of DHF to tetrahydrofolate, Y100 plays an important electrostatic role in modulating the pK_a of the N5 of DHF to enable the preprotonation of DHF by an active site water molecule.

kinetic isotope effect | mechanism | dihydrofolate reductase | synergism

Escherichia coli dihydrofolate reductase (*ec*DHFR) catalyzes the reduction of 7,8-dihydrofolate (DHF) to 5,6,7,8-tetrahydrofolate (THF) through the transfer of a pro*R* hydride from the C4 atom of NADPH to the C6 position of the dihydropterin ring of DHF (1). This enzyme is critical in maintaining the intercellular pool of DHF, which is subsequently used in the biosynthesis of purine nucleotides and some amino acids. Given its biological importance, DHFR is an important drug target (2, 3), and its function has been extensively studied (4–12). However, several fundamental mechanistic details remained incomplete. One unresolved issue is the chronological order of the DHF protonation and hydride transfer steps. Quantum mechanical/molecular mechanical (QM/MM) calculations favor a stepwise protonation-hydride transfer reaction mechanism (10, 13, 14), whereas recent experimental data were interpreted as a change in the reaction mechanism between a concerted process and a stepwise process as a function of pH (15).

The nature of DHF N5 protonation is also not fully understood. D27 has been implicated in the protonation of the N5 position of NADPH (4, 12, 14, 16–18) through a linked water molecule. However, it is not clear how the water molecule-promoted DHF protonation at the N5 of the pterin can change in response to protein conformation (19) and to different electrostatic environments. Recently, the Y100 residue, which is located only *ca.* 3.5 Å from both the amide of the nicotinamide and N8 of the pterin ring (Fig. 1), has been shown to play an important role in electrostatically facilitating the *ec*DHFR-catalyzed reaction (20, 21). The location of Y100 suggests that it may form hydrogen bonds with both ligands to control the distance between them.

Herein, we studied the kinetic behavior of the WT *ec*DHFR and its mutants (D27S, Y100F, and D27S/Y100F) across a much extended pH range, especially with pH > 9. Multiple kinetic isotope effect (KIE) studies across a wide range of pH values found that the WT *ec*DHFR catalyzes the stepwise reduction of DHF, with the protonation of the N5 of DHF preceding the hydride transfer step, through a reaction mechanism that does not change with pH. We also showed that the pK_a of the DHF N5 atom was highly sensitive to changes in the active site electrostatic environment caused by variation in pH (i.e., changes in a protein's ionization state). Specifically, free energy perturbation (FEP) calculations suggest that Y100 can have a large influence on the N5 pK_a so that it can be protonated at alkaline pH. Furthermore, the D27 and Y100 residues function synergistically to provide an active site environment for the solvent-assisted protonation of N5 and to position the reacting substrates, NADPH and DHF, properly.

Results

pL Dependence of WT *ec*DHFR Hydride Transfer Rate. The experimental pH ranges in previous reports were limited to pH 9.5 or lower (1, 6, 15), and upon expanding the experimental conditions to higher pHs, a second plateau was observed (Fig. 2*A*). This finding is consistent with parallel reaction pathways separated by one ionization event (Fig. 3). The hydride transfer rate constant

Significance

Dihydrofolate reductase is a classic drug target because it promotes the NADPH-dependent reduction of 7,8-dihydrofolate (DHF) to yield 5,6,7,8-tetrahydrofolate (THF), which is involved in the biosynthesis of purines, thymidylate, and several amino acids. It is also a popular model system for various biochemical/biophysical studies. However, there are many unresolved mechanistic issues regarding the mechanism of catalysis. We combined primary, solvent, and multiple kinetic isotope effects; their temperature dependence; theoretical calculations; and site-specific mutagenesis to elucidate the reaction mechanism, which involves stepwise protonation of DHF by a water molecule prior to the hydride transfer. These two events are facilitated by two active site residues (D27 and Y100) that operate synergistically to ensure catalysis and to enable efficient DHF protonation over a wide pH range.

Author contributions: C.T.L., K.F., S.H.-S., A.K., and S.J.B. designed research; C.T.L., K.F., J.P.L., and X.H. performed research; C.T.L. contributed new reagents/analytic tools; C.T.L., K.F., J.P.L., X.H., S.H.-S., A.K., and S.J.B. analyzed data; and C.T.L., K.F., S.H.-S., A.K., and S.J.B. wrote the paper.

The authors declare no conflict of interest.

This article is a PNAS Direct Submission.

[1]C.T.L. and K.F. contributed equally to this work.

[2]To whom correspondence may be addressed. Email: amnon-kohen@uiowa.edu or sjb1@psu.edu.

This article contains supporting information online at www.pnas.org/lookup/suppl/doi:10.1073/pnas.1415940111/-/DCSupplemental.

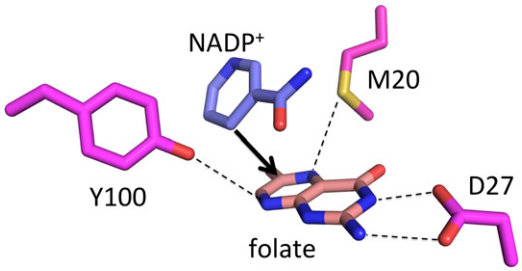

Fig. 1. Orientation of Y100, D27, M20 (magenta), and the ligands in the active site of *ec*DHFR (from Protein Data Bank ID code 1rx2). The black arrow indicates the hydride transfer path.

(k_{hyd}) in the low-pH domain (k_1) is computed to be 830 ± 70 s^{-1} (*SI Appendix*, Table S3), which agrees with the previously determined value of ~950 s^{-1} for the same process (1). The second k_{hyd} rate constant in the high-pH plateau, k_2, is 0.13 ± 0.01 s^{-1}, which is ~6,000-fold lower than k_1. The two pathways are separated by a kinetic pK_a of 6.70 ± 0.05, which is consistent with previously determined values of ~6.5 (1, 5).

A similar sigmoidal relationship was also found for the WT enzyme-catalyzed reaction in D_2O (Fig. 2*A*). The rate/pD profile (pD = −log[D_3O^+]) crosses over once with the rate/pH profile at approximately pL = 7 (pL = −log[H_3O^+] or −log[D_3O^+]). As a result, a normal solvent kinetic isotope effect (SKIE) value was found at low pH (k_1) and an inverse SKIE was found at high pH (k_2) (Table 1). It should be noted that linear relationships were observed in the proton inventory studies in both plateau regions (*SI Appendix*, Fig. S2). This observation is consistent with the involvement of only one proton in the normal SKIEs observed at low pH, but with multiple protons leading to inverse SKIE at high pH (22). Although the SKIE at low pH can be attributed to the protonation of N5 of the DHF, the SKIE at high pH is indicative of the involvement of a whole network of protons in the protonation of N5-DHF. This explanation accords well with the remote effect of protonation of Y100 on D27 and the protonation of N5-DHF discussed below. By that interpretation, many exchangeable protons involved in the network of H-bonds related to the protonation of Y100, D27, and N5-DHF are more tightly bound in the transition state than at the ground state. Based on the fact that the observed 1° KIE was unchanged across the pH range measured, we can rule out the alternative explanation of inverse SKIEs on the DHF binding to the enzyme–NADPH complex (and the associated conformational/protonation states) before the protonation of N5. This mechanism would have led to an inflated commitment (C_f on single-turnover rates) and deflated 1° KIE at higher pH. The observed pH-independent 1° KIE also agrees well with the previously reported values of 2.7–3.0 for the WT *ec*DHFR (1, 13, 15). The data from the multiple isotope effect (23, 24) study (Table 1) show that both SKIE and 1° KIE are suppressed by deuterium substitution at low pH (k_1) but are orthogonal to each other at high pH (k_2).

pL Dependence of D27S and Y100F Mutations. The pL dependence of the k_{hyd} in the D27S, Y100F, and D27S/Y100F mutants was investigated in detail. At pH 7 in water, the rate for the NADPH-dependent reduction of DHF dropped by ~3,400-fold due to the D27S modification (k_{WT} = 279 s^{-1}, k_{D27S} = 0.082 s^{-1}), by ~14-fold due to the Y100F mutation (k_{Y100F} = 19.8 s^{-1}), and more than 100,000-fold with both D27S and Y100F mutations ($k_{Y100F/D27S}$ = 0.0027 s^{-1}). Thus, the rate reduction in the double mutant is greater than the sum of the individual D27S and Y100F effects (i.e., the changes in the free energy barriers of the mutants satisfy the following relation: $\Delta\Delta G^{\ddagger}_{Y100F/D27S} > \Delta\Delta G^{\ddagger}_{Y100F} + \Delta\Delta G^{\ddagger}_{D27S}$, where $G^{\ddagger}$ stands for the activation free energy). All three *ec*DHFR variants (D27S, Y100F, and D27S/Y100F) exhibit linear pL/rate dependence, which differs from the sigmoidal behavior observed in the WT enzyme (Figs. 2 and 4 and *SI Appendix*, Fig. S3). This behavior is true regardless of the identity of the cofactor [β-Nicotinamide adenine dinucleotide phosphate reduced (NADPH) or [Carbonyl-^{14}C]-NADPH, (*R*)-[4-^{3}H]-NADPH (NADPT) and (*R*)-[4-^{2}H]-NADPH (NADPD)] or the solvent (H_2O or D_2O). The slopes for the linear pL/rate relationship were found to be slightly below unity (−0.6 to −0.9). Such nonunity dependencies have been observed before, and they are likely the result of multiple concurrent reaction pathways, each with individual kinetic rate constants (4, 25, 26).

Because there are no plateau regions in the pL/rate profiles for the *ec*DHFR mutants, multiple isotope effect analyses (23, 24) were conducted at specific pL values of 5.1, 6.0, 7.0, and 8.2 (*SI Appendix*, Table S2). The Y100F mutant exhibited an inverse SKIE at high pH, and the SKIE progressively increased to slightly above unity as the pH was lowered to 5.1. Conversely, the primary KIE value starts at ~3.2–3.3 at pH 8.2, but it progressively decreases in magnitude in going to lower pHs. For the D27S and D27S/Y100F mutants, inverse SKIE values were found between pH 5.1 and pH 8.2, and the magnitude of the SKIE stayed constant. Similarly, the 1° KIE values on the hydride transfer reaction in these two *ec*DHFR mutants are ~2.7 and insensitive to pL changes.

Temperature Dependence of Intrinsic KIEs for Y100F, D27S, and Y100F/D27S *ec*DHFRs. Competitive hydrogen to deuterium (H/D) and hydrogen to tritium (H/T) KIEs on the second-order rate constant (k_{cat}/K_m) were measured for each variant of *ec*DHFR to assess the intrinsic KIE on the catalyzed hydride transfer. The intrinsic KIEs for each mutant are temperature-dependent, as evident from the nonzero isotope effects on the activation energy (ΔE_{aH-D}) (Table 2). These results are very different from the temperature-independent intrinsic KIE of the WT enzyme (27), suggesting a role for each residue in the catalyzed hydride transfer. A comparison of the ΔE_{aH-D} values of the Y100F and D27S single mutants with the ΔE_{aH-D} value of the D27S/Y100F double mutant indicates greater than additive behavior (Table 2; $\Delta E_{aH-D\mathrm{D27/Y100}} > \Delta E_{aH-D\mathrm{Y100F}} + \Delta E_{aH-D\mathrm{D27S}}$), suggesting the residues act synergistically.

Calculation of Relative pK_a Values at Position N5 of DHF. FEP calculations were used to calculate the free energy for deprotonating the N5 position of DHF with neutral Y100 relative to anionic Y100 (i.e., when the hydroxyl group is deprotonated). The pK_a of the N5 of DHF has been measured (1, 16) and calculated (12, 19) to be between 6.5 and 7. The calculated difference in the Helmholtz free energies of deprotonation for the two protonation states of Y100 is $\Delta\Delta A^{FEP}$ = 6.08 ± 0.92 kcal·mol^{-1}, corresponding to a pK_a shift of 4.7 units (Table 3). The hydride

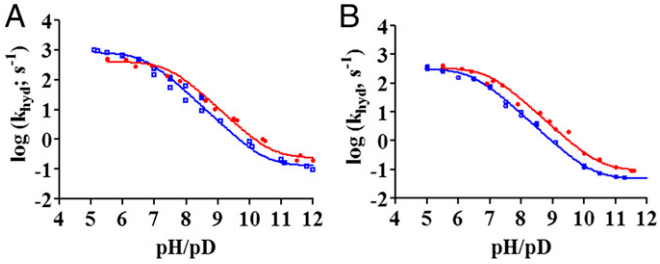

Fig. 2. Log k_{hyd} vs. pH/pD for the WT *ec*DHFR at 25 °C with NADPH in H_2O (blue □) and NADPH in D_2O (red ●) (*A*) and NADPD in H_2O (blue □) and NADPD in D_2O (red ●) (*B*). The data points were fit to *SI Appendix*, Eq. **S1**, and the rate constants are summarized in *SI Appendix*, Table S2.

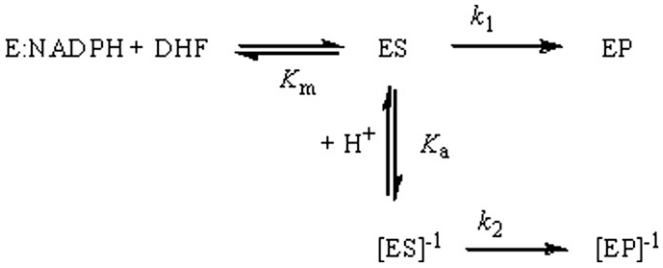

Fig. 3. Proposed reaction scheme for the *ec*DHFR-promoted hydride transfer reaction with parallel pathways. EP, enzyme/products complex; ES, ternary enzyme/substrate Michaelis–Menten complex.

donor-acceptor distances from our molecular dynamics (MD) simulations are the same to within the statistical accuracy when the Y100 hydroxyl group is deprotonated or protonated.

Discussion

DHFR is one of the most well-studied enzyme systems and is commonly used as a model system for biochemical/biophysical inquiries. Although much is known about its catalytic cycle, inhibition characteristics, and structural dynamics, many mechanistic details regarding the chemical step of catalysis (DHF→THF) are still unresolved. This situation is troubling because the numerous mutagenesis studies that examine how the chemical step is being affected by specific mutations remain incomplete. Without a comprehensive understanding of the reaction mechanism, it is difficult to attribute the kinetic effect of the mutation(s) definitively.

To gain further mechanistic understanding, we first extended the pH range of the experimental conditions and found sigmoidal-shaped pH/rate profiles (Fig. 2), which are consistent with two parallel reaction pathways consisting of the ternary enzyme/substrate (ES) Michaelis–Menten complex and the associated deprotonated form, ES^{-1} (separated by one ionization step). Although multiple *ec*DHFR ternary/binary complexes in solution have been reported (28), two catalytically competent ternary complexes, separated by protein ionization, were unknown (*SI Appendix*, Fig. S4). Also, the origin of the activity change with a pK_a of 6.5 had drawn several interpretations. The data here show that there is a second catalytic complex that exists predominantly at higher pH and is capable of converting DHF into THF, albeit with a much lower rate constant. The kinetic pK_a determined from the pH/rate profiles is associated with an ionization event that is related to the interconversion between these two reactive complexes (Fig. 3 and *SI Appendix*, Eq. **S1**), and not necessarily related to a change in the order or timing of DHF-N5 protonation and hydride transfer. As a consequence, the system will contain different ratios of the two reactive species at the various pH values in Fig. 2. It should be noted that the presence of two reactive ternary complexes that occupy the high- and low-pH domains has been hinted at in a recent study (G51PEKN, N23PP/G51PEKN, and N23PP/L28F/G51PEKN *ec*DHFR mutants) (5), but the implications were unclear at that point.

Because the reduction of DHF involves both proton transfer to its N5 and hydride transfer to C6, examination of the cross-effects of 1° KIEs (probing the hydride transfer) and SKIEs (probing the protonation step) is useful for dissecting the timing of these two processes. If protonation and hydride transfer occur simultaneously in a concerted mechanism (middle mechanism in Fig. 5 and *SI Appendix*, Fig. S5, *Bottom*), the observed 1° KIE should increase in deuterated solvent because the deuterium would increase the energy barrier for the hydride transfer event, making it more rate-limiting (24). Thus, the data in Table 1 are inconsistent with a concerted mechanism. At low pH, both 1° KIE and SKIE are suppressed by deuterium in the other step. At high pH, on the other hand, the 1° KIEs and the SKIEs are unchanged by D_2O and NADPD, respectively, suggesting those observed KIEs are not masked by deuterium in the other step. These data are consistent with a stepwise mechanism illustrated in *SI Appendix*, Fig. S5 (*Upper*). Previously it was suggested, based on KIEs, that the reaction mechanism might shift to a concerted process at a higher pH of 9.5 (15). However, this assessment overlooked the fact (24) that in this case, the inverse SKIEs at high pH would suppress a 1° KIE for a concerted process. That behavior was not observed. More importantly, a shift to a concerted mechanism would mean that the rate of the reaction would continuously drop by 10-fold for every pH unit increase, which is inconsistent with the high-pH plateau in Fig. 2.

There are two potential stepwise mechanisms, shown in Fig. 5 (*Top* and *Bottom*), and they differ in the chronological ordering of events. The kinetic observable, oxidation of NADPH, may capture both the isotope effects on the hydride transfer and proton transfer. If hydride transfer occurs before the protonation step in a stepwise mechanism (Fig. 5, *Top*), one should find a nonunity 1° KIE and no significant SKIE effect (SKIE = 1) because the solvent-assisted protonation step would be after the kinetic observable (loss of NADPH fluorescence energy transfer). Table 1 shows that this situation is not the case, suggesting that the actual mechanism involves N5-DHF protonation preceding the hydride transfer (Fig. 5, *Bottom*).

The second ternary complex that exists at high pH is much less reactive, with its free energy barrier for DHF reduction being ~5.2 kcal/mol higher than the free energy barrier for DHF reduction for the more reactive species. This change could cause the kinetic expression to shift from a steady-state approximation (low pH; *SI Appendix*, Eq. **S7**) to one that involves a preequilibrium approximation (high pH; *SI Appendix*, Eq. **S8**). In other words, when the $k_{hyd} << k_{prot}'$ (protonation rate), the steady-state expression would simplify into a preequilibrium approximation. This interpretation is consistent with the observed inverse SKIE at high pH, which is indicative of a preequilibrium step. The inverse SKIE can then be attributed to the acid/base equilibrium of DHF being affected by the higher acidity of D_2O compared with H_2O (29, 30). Under comparable conditions, a higher concentration of the DHF-H^+/D^+ intermediate will be formed in

Table 1. SKIE and 1° KIEs in the plateau regions of the WT *ec*DHFR hydride transfer pL/rate profiles

pH region	SKIE (NADPH)	SKIE (NADPD)	KIE (H_2O)	KIE (D_2O)
Low pH (k_1)	2.0 ± 0.2	0.9 ± 0.1	2.6 ± 0.3	1.2 ± 0.1
High pH (k_2)	0.57 ± 0.09	0.53 ± 0.08	2.7 ± 0.3	2.6 ± 0.4

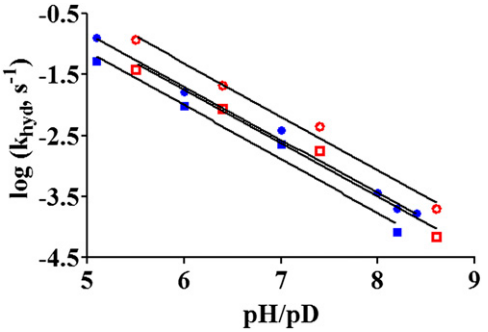

Fig. 4. Log (k_{hyd}) vs. pH/pD for the D27S/Y100F *ec*DHFR mutant at 25 °C. The data points are presented as NADPH in H_2O (●) and NADPH in D_2O (○) and NADPD in H_2O (■) and NADPD in D_2O (□). The parameters used for the fitted linear lines are given in *SI Appendix*, Table S1.

Table 2. Parameters from regression of intrinsic H/D 1° KIE_{int} data to Arrhenius equation

DHFR	A_H/A_D	ΔE_{aH-D}, kcal/mol
WT, pH 7.0	2.83 ± 0.66	0.03 ± 0.04
WT, pH 9.0	3.61 ± 0.86	−0.01 ± 0.23
Y100F	3.35 ± 0.13	0.24 ± 0.02
D27S	1.41 ± 0.09	0.76 ± 0.04
D27S/Y100F	0.10 ± 0.01	2.25 ± 0.09

A_D, Arrhenius constant for D; A_H, Arrhenius equation for H.

D_2O, relative to H_2O, resulting in a larger observed rate (k_{hyd} * [DHF-D^+]). It should be pointed out that global effects of higher medium viscosity (D_2O) and increased protein rigidity (N − D = O hydrogen bonds) have been ruled out as the cause for the inverse SKIE data in *ec*DHFR (15).

The relationships between the observed KIEs on WT enzyme k_{hyd} and their intrinsic values further support the above interpretations. The temperature dependence of the intrinsic KIEs is pH-independent (zero at both high and low pH), which further supports our conclusion that the C-H→C hydride transfer step, per se, is not concerted with the protonation step in either pH range. The data clearly reveal that the differences between the temperature-independent deuteride transfer rate constant $^Dk_{hyd}$ at pH 9 (*SI Appendix*, Fig. S1*A*) and temperature-dependent $^Dk_{hyd}$ at pH 7 (*SI Appendix*, Fig. S1*B*) actually result from a pH-dependent commitment to catalysis on the k_{hyd} (*C* in *SI Appendix*, Eq. **S6**). The likely explanation for these findings is that the commitment in the DHF protonation step reflects the steady-state and equilibrium approximations for the fraction of protonated DHF in the reactive Michaelis–Menten complex committed to the C-H→C hydride transfer.

We also examined the roles of two active site residues, D27 and Y100, which might play a role in the protonation step and the positioning of the substrates and water molecules for the subsequent hydride transfer, based on crystal structures and computer simulations. D27 has been shown in previous studies to be important for facilitating a solvent-assisted proton delivery to the N5 position of DHF, thus generating the protonated substrate for the subsequent hydride transfer (4, 16–18, 31). The direct source of the proton is likely to be a water molecule that could enter the active site as the Met20 loop changes conformations (18), and crystal data supporting this hypothesis are provided in the accompanying work by Wan et al. (32). Y100 has been implicated to provide electrostatic stabilization of the developing positive charge on the nicotinamide moiety, as well as exhibiting strong electrostatic interactions with $NADP^+$ and folate (20, 21).

Mutagenesis studies show that the D27S, Y100F, and D27S/Y100F mutants all exhibit linear pH/rate profiles with no indication of a plateau region in either the low- or high-pH regions (Fig. 4 and *SI Appendix*, Fig. S3). This disruption of the WT pH dependence observed suggests that these two residues are important for the proton transfer to DHF. Through appropriate electrostatic interactions with the substrate and cofactor, Y100 and D27 provide optimal conditions for the solvent-assisted proton transfer step of the reaction (4, 7, 18, 20). In all mutants, 1° KIE values above unity were found (*SI Appendix*, Table S2). Inverse SKIE values were found in all cases across the probed pH range, which indicates a preequilibrium protonation of DHF in a stepwise mechanism for the reduction of DHF. Thus, the mutations lead to a suboptimal catalytic environment but do not alter the sequence of protonation followed by hydride transfer. Whereas the D27S mutation induces a greater catalytic penalty than the Y100F mutation, the rate reduction observed in the D27S/Y100F double mutation is greater than the sum of the respective effects of the individual mutations (i.e., $\Delta\Delta G^{\ddagger}_{Y100F/D27S} > \Delta\Delta G^{\ddagger}_{Y100F} + \Delta\Delta G^{\ddagger}_{D27S}$; *SI Appendix*, Table S4), strongly suggesting a synergistic function of these two residues.

The role of Y100 and D27 in the hydride transfer step (just C-H→C) was further investigated through the temperature dependence of the intrinsic 1° KIEs, and our findings support the synergism of D27/Y100. As shown by several theoretical (33–36) and experimental (9) studies, the temperature dependence of intrinsic KIEs is sensitive to changes in the hydride donor-acceptor distance fluctuations. Fig. 6 and Table 2 indicate that each single mutant not only has a larger temperature dependence of intrinsic KIEs than the WT enzyme but also that the effect of the double mutant is more than additive (Table 2; $\Delta E_{a\ Y100F/D27S} > \Delta E_{a\ Y100F} + \Delta E_{a\ D27S}$). Replacing either Y100 or D27 resulted in inflated and more temperature-dependent intrinsic KIEs on hydride transfer, suggesting that these residues play a role in the narrow donor-acceptor distance distribution of the WT.

An interesting question regarding the second catalytic competent E:NADPH:DHF complex in the high-pH domain is the protonation of N5 to generate the reactive species for the hydride transfer event (here E refers to the enzyme). If the pK_a of the N5 stayed constant at ∼6.5 (1, 12, 16), there would not be sufficient concentration of the reactive species E:NADPH:DHF-H^+ in the high-pH domain for the subsequent hydride transfer reaction to occur at the observed rate. In fact, under single-turnover conditions (3 μM total ternary species), the second-order rate constant to protonate and achieve the observed k_2 value (0.13 s^{-1}) in the high-pH plateau region of Fig. 2*A* (WT enzyme, NADPH, and H_2O) from E:NADPH:DHF would be above the diffusion-controlled limit for a biomolecular process in water (37) (∼4× diffusion limit at pH 12). Because it is known that the N5 pK_a can fluctuate (up to ∼9) depending on the active site conformation (19), it is reasonable to speculate that structural rearrangement will impose a change in the active site electrostatics, which might affect N5 acidity. We focused on the effect of the Y100 residue, a high-pK_a residue close to the reactive center, and found that the deprotonation of Y100 alone can greatly perturb the N5 pK_a by ∼4.7 units (i.e., up to ∼11.2; Table 3). Therefore, a more anionic active site environment (with Y100/other residues deprotonated/partially deprotonated) could increase the N5 pK_a to ensure sufficient DHF protonation under alkaline conditions.

Conclusion

The mechanistic details of both proton and hydride transfers in the reaction catalyzed by *ec*DHFR have been elucidated through multiple isotope effects (SKIEs on 1° KIEs) (23, 24) over a broader pH range than has been previously studied. Whereas the measured rates and KIEs at the pH range of 7–9 were the same

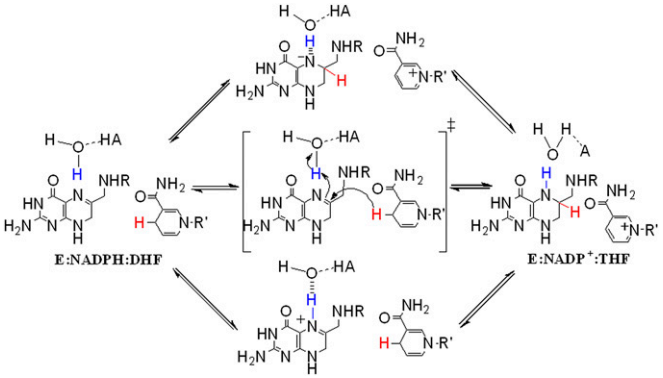

Fig. 5. Potential mechanistic pathways for the WT *ec*DHFR proton and hydride transfer reactions.

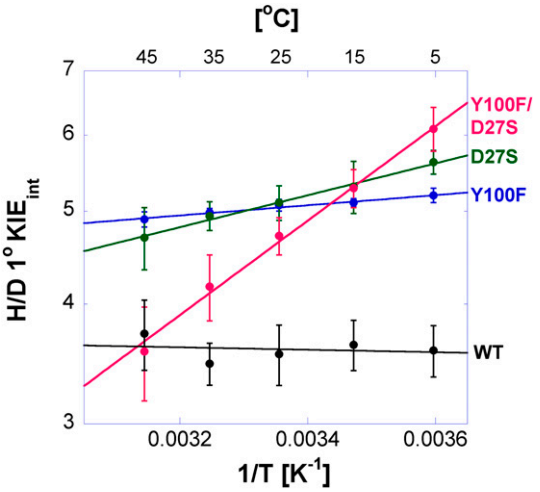

Fig. 6. Arrhenius plots of the intrinsic H/D KIEs of the hydride transfer reaction catalyzed by WT (black) (27), Y100F (blue), D27S (green), and D27S/Y100 (magenta) *ec*DHFRs.

as reported (1, 6, 15), the broader pH range revealed a previously unidentified catalytically active ternary complex that exists predominantly at high pH. The data at both low and high pH support a stepwise mechanism in which protonation of the N5 atom of DHF precedes the reduction of a DHF-H^+ intermediate by NADPH and no mechanistic shift as a function of pH.

Also, the active site D27 and Y100 residues play an important and synergistic role in facilitating both the proton transfer and hydride transfer steps. Mutations of D27, Y100, or both disrupt the sigmoidal pH/rate dependence observed in the WT. The protonation of DHF is likely to occur through a water molecule, as shown by the accompanying crystallographic data by Wan et al. (32), whereas the D27 and Y100 residues may help to orient the substrates and the water molecule through various electrostatic interactions. Further evidence of the important role of Y100 was obtained from FEP calculations of the pK_a of DHF N5. These calculations indicate that the N5 pK_a might be significantly altered by the active site electrostatics via the ionization state of residues, such as Y100, to ensure that DHF can be efficiently protonated before the hydride transfer event.

These findings provide an important validation for computational simulations concluding that protonation of DHF occurs before the transfer of a hydride, and further justify approaches that assumed a protonated DHF for simulating the free energy barriers for the hydride transfer reactions of *ec*DHFR/*ec*DHFR mutants (10–13, 38). Furthermore, the results here provide additional insights on how *ec*DHFR catalysis might be affected by pH, which could induce large effects on active site ionization states and electrostatics. Because *ec*DHFR catalysis has emerged as a popular model system for enzyme-catalyzed reactions, a better understanding of its reaction mechanism may have a broad impact on enzymology in general.

Materials and Methods

***ec*DHFR Variants.** Y100F, D27S, and D27S/Y100F *ec*DHFR variants were constructed using the Stratagene QuikChange site-directed mutagenesis kit and the WT *ec*DHFR template as described (39). Primer sequences were 5′-CA TGG AAC CTG CCT GCC AGT CTC GCC TGG TTT AAA CGC -3′ (D27S) and 5′-GGC GGC GGA CGC GTT TTT GAA CAG TTC TTG CC-3′ (Y100F). Plasmid construction, protein expression, and purification of mutant DHFRs were performed according to the published protocols (39).

Kinetics. All reactions were performed following a published protocol in MTEN [2-(N-morpholino)ethanesulfonic acid:2-Amino-2-hydroxymethyl-propane-1,3-diol:ethanolamine] buffer adjusted to various pH values (with HCl/NaOH) (1). Presteady-state kinetics were done under either single-turnover or excess substrate conditions using an Applied Photophysics stopped-flow spectrophotometer at 25 °C. Both conditions yielded the same rate, indicating that at the concentration of 3 μM, DHF is completely bound to the E:NADPH binary complex within the mixing dead-time of the instrument. Under single-turnover conditions, 10 μM enzyme, 200 μM NADPH, 2 mM DTT, and 50 mM MTEN buffer were loaded into one of the stopped-flow syringes, whereas the other syringe held 6–8 μM DHF, 2 mM DTT, and 50 mM MTEN buffer. Upon mixing, the initial concentrations of the individual species in the reaction chamber were halved. The excess substrate conditions (burst kinetics in a multiple turnover experiment) used 20 μM enzyme, 250 μM NADPH, 2 mM DTT, and 50 mM MTEN buffer in one stopped-flow syringe. The other syringe held 200 μM DHF, 2 mM DTT, and 50 mM MTEN buffer. The reaction mixture was excited at 290 nm, and the emission was measured using a 400-nm cutoff output filter for the loss of FRET from the enzyme to NADPH (1). The fluorescence over time traces (of the burst phase under excess substrate conditions) were fit to a standard single exponential expression to determine k_{hyd}. The k_{hyd} values at various pL values (pH/pD) are averages of five separate kinetic runs. Primary KIE measurements in which NADPH was substituted with NADPD were conducted according to the concentrations and conditions listed above. Detailed data analyses are described in *SI Appendix*.

SKIE. Separate stock solutions of NADPH/NADPD, DHF, and DTT were prepared in D_2O. MTEN buffers in D_2O (0.5 M) at various pD values were also prepared. The enzymes were buffer-exchanged into a 50 mM phosphate buffer prepared in D_2O. The final experimental concentrations and the conditions were similar to the experimental concentrations and conditions described above. Under the concentrations used for stopped-flow kinetic experiments, the [H_2O] to [D_2O] + [H_2O] ratio was less than 5% (vol/vol). Separate proton inventory studies were performed under the excess substrate conditions. The proton inventory studies were performed with 0%, 20%, 40%, 50%, 60%, 80%, and 100% (vol/vol) D_2O/H_2O at 25 °C. A standard linear expression was used to fit the kinetic data.

Competitive KIEs. Intrinsic KIEs were determined from H/T and D/T KIEs on the second-order rate constant (k_{cat}/K_M) measured by a competitive assay following published procedures (40, 41). In short, purified radiolabeled NADPH with 4*R*-T (tritium at position 4*R* of NADPH) and Ad-^{14}C (^{14}C on the adenine base of NADPH) was mixed at a 5:1 ^{3}H/^{14}C ratio to measure 1° KIEs for either H/T (where the Ad-^{14}C traced 4*R*-H) or H/D (where the Ad-^{14}C traced 4*R*-D) ratios. The mixtures were copurified by reverse-phase HPLC, divided into aliquots containing at least 300,000 dpm of ^{14}C, and flash-frozen in liquid nitrogen for storage at −80 °C. KIEs were then measured in MTEN buffer at 5–45 °C. Each reaction mixture contained 0.85 mM DHF and 4 μM radiolabeled NADPH. The reactions were quenched at various time points by addition of methotrexate, mixed, and immediately frozen on dry ice. Samples were thawed before HPLC analysis and bubbled with oxygen for 12 min to oxidize the THF product. Resolution of the reaction mixture was achieved by HPLC using a published method (42), and the fractions were counted by liquid scintillation analysis. Detailed data analysis is provided in *SI Appendix*.

FEP pK_a Calculations. The relative pK_a of the N5 position of DHF was determined using FEP calculations (43) for the protonated and deprotonated hydroxyl groups of Y100 using the GROMACS program (44). In both cases, the rest of the titratable enzyme residues were assigned protonation states that corresponded to pH 7. MD trajectories were propagated for a series of intermediate states between the protonated (DHF-H^+) and deprotonated

Table 3. Calculated free energy for deprotonation and associated pK_a at the N5 of DHF bound in the closed form of *ec*DHFR

Property	Y100 protonated	Y100 deprotonated
Δ*A*, kcal/mol	−11.41 ± 0.42	−5.33 ± 0.82
pK_a	6.5*	11.2
<D–A>, Å	3.7 ± 0.2	3.6 ± 0.2

A, Helmholtz free energy; A, acceptor; D, donor; <D–A>, average hydride donor-acceptor distance.
*Value obtained from ref. 1.

(DHF) substrates. We used a λ-dynamics methodology, where λ defines a potential energy function between two different states A and B:

$$U(\lambda) = (1-\lambda)U_A + \lambda U_B,$$

where state A corresponds to protonated DHF (DHF-H^+) and state B corresponds to an analog of DHF with a dummy particle bonded at the N5 position. The effective partial charges for the DHF substrate are varied as a function of λ for the intermediate windows.

For each system studied, nine intermediate windows were generated (λ = 0.0, 0.1, 0.2, 0.3, 0.5, 0.7, 0.8, 0.9, and 1.0). The system was equilibrated in state A, followed by an additional 1 ns of equilibration for each window before propagating for 10 ns per window for a total of 90 ns per dataset. The free energy was calculated as a function of λ using the *g_bar* utility in GROMACS, and the free energy of DHF-H^+ deprotonation was calculated using the Bennett acceptance ratio method (45). These free energies are Helmholtz energies, denoted *A*, because they are calculated in the canonical (constant number of particles, volume, and temperature) ensemble. We calculated the relative free energies because state B in our FEP scheme does not correspond exactly to the deprotonated DHF, and this systematic error approximately cancels in the calculation of relative free energies. For each protonation state of Y100, a second dataset yielded values within 1.0 kcal·mol^{-1}. Additional details are provided in *SI Appendix*.

ACKNOWLEDGMENTS. This work was supported by National Science Foundation Grant 1149023 and NIH Grants GM65368 (to A.K.), GM056207 (to J.P.L. and S.H.-S.), and GM092946 (to C.T.L., X.H., and S.J.B.). C.T.L. acknowledges a postdoctoral fellowship from the Natural Sciences and Engineering Research Council of Canada.

1. Fierke CA, Johnson KA, Benkovic SJ (1987) Construction and evaluation of the kinetic scheme associated with dihydrofolate reductase from Escherichia coli. *Biochemistry* 26(13):4085–4092.
2. Purcell WT, Ettinger DS (2003) Novel antifolate drugs. *Curr Oncol Rep* 5(2):114–125.
3. Sasso SP, Gilli RM, Sari JC, Rimet OS, Briand CM (1994) Thermodynamic study of dihydrofolate reductase inhibitor selectivity. *Biochim Biophys Acta* 1207(1):74–79.
4. Howell EE, Villafranca JE, Warren MS, Oatley SJ, Kraut J (1986) Functional role of aspartic acid-27 in dihydrofolate reductase revealed by mutagenesis. *Science* 231(4742):1123–1128.
5. Liu CT, et al. (2013) Functional significance of evolving protein sequence in dihydrofolate reductase from bacteria to humans. *Proc Natl Acad Sci USA* 110(25): 10159–10164.
6. Loveridge EJ, Allemann RK (2011) Effect of pH on hydride transfer by Escherichia coli dihydrofolate reductase. *ChemBioChem* 12(8):1258–1262.
7. Sawaya MR, Kraut J (1997) Loop and subdomain movements in the mechanism of Escherichia coli dihydrofolate reductase: Crystallographic evidence. *Biochemistry* 36(3):586–603.
8. Schnell JR, Dyson HJ, Wright PE (2004) Structure, dynamics, and catalytic function of dihydrofolate reductase. *Ann Rev Biophys Biomol Struct* 33:119–140.
9. Stojković V, Perissinotti LL, Willmer D, Benkovic SJ, Kohen A (2012) Effects of the donor-acceptor distance and dynamics on hydride tunneling in the dihydrofolate reductase catalyzed reaction. *J Am Chem Soc* 134(3):1738–1745.
10. Castillo R, Andres J, Moliner V (1999) Catalytic mechanism of dihydrofolate reductase enzyme. A combined quantum-mechanical/molecular-mechanical characterization of transition state structure for the hydride transfer step. *J Am Chem Soc* 121(51): 12140–12147.
11. Pu J, Ma S, Gao J, Truhlar DG (2005) Small temperature dependence of the kinetic isotope effect for the hydride transfer reaction catalyzed by Escherichia coli dihydrofolate reductase. *J Phys Chem B* 109(18):8551–8556.
12. Rod TH, Brooks CL III (2003) How dihydrofolate reductase facilitates protonation of dihydrofolate. *J Am Chem Soc* 125(29):8718–8719.
13. Agarwal PK, Billeter SR, Hammes-Schiffer S (2002) Nuclear quantum effects and enzyme dynamics in dihydrofolate reductase catalysis. *J Phys Chem B* 106(12):3283–3293.
14. Ferrer S, Silla E, Tuñón I, Tuñón I, Moliner V (2003) Catalytic mechanism of dihydrofolate reductase enzyme. A combined quantum-mechanical/molecular-mechanical characterization of the N5 protonation step. *J Phys Chem B* 107(50):14036–14041.
15. Loveridge EJ, Behiry EM, Swanwick RS, Allemann RK (2009) Different reaction mechanisms for mesophilic and thermophilic dihydrofolate reductases. *J Am Chem Soc* 131(20):6926–6927.
16. Chen YQ, Kraut J, Blakley RL, Callender R (1994) Determination by Raman spectroscopy of the pKa of N5 of dihydrofolate bound to dihydrofolate reductase: Mechanistic implications. *Biochemistry* 33(23):7021–7026.
17. David CL, et al. (1992) Structure and function of alternative proton-relay mutants of dihydrofolate reductase. *Biochemistry* 31(40):9813–9822.
18. Shrimpton P, Allemann RK (2002) Role of water in the catalytic cycle of E. coli dihydrofolate reductase. *Protein Sci* 11(6):1442–1451.
19. Khavrutskii IV, Price DJ, Lee J, Brooks CL III (2007) Conformational change of the methionine 20 loop of Escherichia coli dihydrofolate reductase modulates pKa of the bound dihydrofolate. *Protein Sci* 16(6):1087–1100.
20. Groff D, Thielges MC, Cellitti S, Schultz PG, Romesberg FE (2009) Efforts toward the direct experimental characterization of enzyme microenvironments: Tyrosine100 in dihydrofolate reductase. *Angew Chem Int Ed Engl* 48(19):3478–3481.
21. Liu CT, et al. (2014) Probing the electrostatics of active site microenvironments along the catalytic cycle for Escherichia coli dihydrofolate reductase. *J Am Chem Soc* 136(29):10349–10360.
22. Quinn DM (2005) Theory and practice of solvent isotope effects. *Isotope Effects in Chemistry and Biology*, eds Kohen A, Limbach HH (Taylor & Francis, CRC Press, Boca Raton, FL), Vol 41, pp 995–1018.
23. Belasco JG, Albery WJ, Knowles JR (1983) Double isotope fractionation Test for concertedness and for transition-state dominance. *J Am Chem Soc* 105(8):2475–2477.
24. Hermes JD, Roeske CA, O'Leary MH, Cleland WW (1982) Use of multiple isotope effects to determine enzyme mechanisms and intrinsic isotope effects. Malic enzyme and glucose-6-phosphate dehydrogenase. *Biochemistry* 21(20):5106–5114.
25. Czekster CM, Vandemeulebroucke A, Blanchard JS (2011) Two parallel pathways in the kinetic sequence of the dihydrofolate reductase from Mycobacterium tuberculosis. *Biochemistry* 50(32):7045–7056.
26. Hammes GG, Benkovic SJ, Hammes-Schiffer S (2011) Flexibility, diversity, and cooperativity: Pillars of enzyme catalysis. *Biochemistry* 50(48):10422–10430.
27. Sikorski RS, et al. (2004) Tunneling and coupled motion in the Escherichia coli dihydrofolate reductase catalysis. *J Am Chem Soc* 126(15):4778–4779.
28. Zhang Z, Rajagopalan PTR, Selzer T, Benkovic SJ, Hammes GG (2004) Single-molecule and transient kinetics investigation of the interaction of dihydrofolate reductase with NADPH and dihydrofolate. *Proc Natl Acad Sci USA* 101(9):2764–2769.
29. Czekster CM, Vandemeulebroucke A, Blanchard JS (2011) Kinetic and chemical mechanism of the dihydrofolate reductase from Mycobacterium tuberculosis. *Biochemistry* 50(3):367–375.
30. Wiberg KB (1955) The deuterium isotope effect. *Chem Rev* 55(4):713–743.
31. Dunn SM, Lanigan TM, Howell EE (1990) Dihydrofolate reductase from Escherichia coli: Probing the role of aspartate-27 and phenylalanine-137 in enzyme conformation and the binding of NADPH. *Biochemistry* 29(37):8569–8576.
32. Wan Q, et al. (2014) Toward resolving the catalytic mechanism of dihydrofolate reductase using neutron and ultrahigh-resolution X-ray crystallography. *Proc Natl Acad Sci USA* 111:18225–18230.
33. Antoniou D, Caratzoulas S, Kalyanaraman C, Mincer JS, Schwartz SD (2002) Barrier passage and protein dynamics in enzymatically catalyzed reactions. *Eur J Biochem* 269(13):3103–3112.
34. Hammes-Schiffer S (2006) Hydrogen tunneling and protein motion in enzyme reactions. *Acc Chem Res* 39(2):93–100.
35. Hay S, Sutcliffe MJ, Scrutton N (2009) Probing coupled motions in enzymatic hydrogen tunnelling reactions: Beyond temperature-dependence studies of kinetic isotope effects. *Quantum Tunnelling in Enzyme-Catalyzed Reactions*, eds Allemann R, Scrutton N (Royal Society of Chemistry, London, UK), pp 199–218.
36. Klinman JP, Kohen A (2013) Hydrogen tunneling links protein dynamics to enzyme catalysis. *Annu Rev Biochem* 82(1):471–496.
37. Keizer J (1987) Diffusion effects on rapid bimolecular chemical-reactions. *Chem Rev* 87(1):167–180.
38. Liu H, Warshel A (2007) Origin of the temperature dependence of isotope effects in enzymatic reactions: The case of dihydrofolate reductase. *J Phys Chem B* 111(27): 7852–7861.
39. Cameron CE, Benkovic SJ (1997) Evidence for a functional role of the dynamics of glycine-121 of Escherichia coli dihydrofolate reductase obtained from kinetic analysis of a site-directed mutant. *Biochemistry* 36(50):15792–15800.
40. Francis K, Stojkovic V, Kohen A (2013) Preservation of protein dynamics in dihydrofolate reductase evolution. *J Biol Chem* 288(50):35961–35968.
41. Sen A, Yahashiri A, Kohen A (2011) Triple isotopic labeling and kinetic isotope effects: Exposing H-transfer steps in enzymatic systems. *Biochemistry* 50(29):6462–6468.
42. Markham KA, Sikorski RS, Kohen A (2004) Synthesis and utility of ^{14}C-labeled nicotinamide cofactors. *Anal Biochem* 325(1):62–67.
43. Hansen N, van Gunsteren WF (2014) Practical aspects of free-energy calculations: A review. *J Chem Theory Comput* 10(7):2632–2647.
44. Hess B, Kutzner C, van der Spoel D, Lindahl E (2008) GROMACS 4: Algorithms for highly efficient, load-balanced, and scalable molecular simulation. *J Chem Theory Comput* 4(3):435–447.
45. Bennett CH (1976) Efficient estimation of free-energy differences from Monte-Carlo data. *J Comput Phys* 22(2):245–268.